Atmospheric Environment Vol. 22, No. 9, pp. 1985 2001, 1988.
Printed in Great Britain.

0004-6981/88 $3.00+0.00

DEVELOPMENT AND EVALUATION OF AN EULERIAN PHOTOCHEMICAL GAS–AEROSOL MODEL

CHRISTODOULOS PILINIS
Environmental Quality Laboratory, California Institute of Technology, Pasadena, CA 91125, U.S.A.

and

JOHN H. SEINFELD
Department of Chemical Engineering, California Institute of Technology, Pasadena, CA 91125, U.S.A.

(*First received* 12 *November* 1987 *and in final form* 19 *February* 1988)

Abstract—A three-dimensional Eulerian model that simulates the concentrations of gaseous pollutants and the size–composition distribution of multicomponent atmospheric aerosols has been developed and used to study the evolution of the aerosol-size distribution and composition in the South Coast Air Basin of California. The predictions of the model are compared with ambient measurements of sulfate, nitrate, sodium, chloride and ammonium aerosol.

Key word index: Aerosols, mathematical model, organic aerosols.

INTRODUCTION

To predict atmospheric aerosol size and composition, it is necessary to account for gas-phase processes that lead to aerosol products, transport of gases to the surfaces of particles, formation of new particles by nucleation, shaping of the size distribution by coagulation and equilibration of particles with the local gaseous environment. Aerosols in the polluted urban atmosphere can be considered to consist of a mixture of sulfates, nitrates, water, ammonium, elemental and organic carbon and dust (Fig. 1). Primary particles are emitted and advected from their sources by the wind, while gas-phase, photochemical reactions occur, converting NO_x to nitric acid (HNO_3), SO_2 to sulfuric acid (H_2SO_4) and reactive organic gases to low-vapor-pressure, condensable species. Water vapor is ubiquitous, and ammonia is generally also present in the gas phase. Gas-to-particle conversion of sulfate, nitrate, ammonium and organics may occur as these gas-phase reactions proceed, either by homogeneous nucleation or condensation on existing particles.

In previous work (Pilinis *et al.*, 1987) we have shown that non-equilibrium aerosol growth and coagulation, coupled with continuous reestablishment of gas- and particulate-phase chemical equilibrium, predicts the key features of the evolution of the urban aerosol size–composition distribution. We have also demonstrated the importance of ionic species, especially sodium, in shaping the aerosol size distribution, as well as in determining the nitrate concentration in the particulate phase (Pilinis and Seinfeld, 1987).

In this work we present an Eulerian, three-dimensional urban airshed atmospheric aerosol model that represents a merging of a three-dimensional Eulerian, gas-phase, air-quality model (McRae *et al.*, 1982a) with the aerosol models developed by Pilinis and Seinfeld (1987). We begin with a description of the full Eulerian model, followed by a listing of its input data requirements. We then apply the model to simulate the aerosol evolution in the Los Angeles basin on 30 August 1982, and we conclude with a brief statistical evaluation of the model performance.

MODEL DESCRIPTION

The size and composition of particles undergoing nucleation, condensation, coagulation, transport and deposition are governed by the aerosol general dynamic equation (Seinfeld, 1986). The sectional approximation of this equation, in which the continuous size distribution is approximated by a series of step functions, is particularly advantageous for numerical solution of the equation (Warren and Seinfeld, 1985; Pilinis *et al.*, 1987). The evolution of the mass concentration of species i in the lth section, Q_{il}, is described by the following integrated form of the general dynamic equation:

$$\frac{\partial Q_{il}}{\partial t}+\nabla\cdot(\mathbf{u}Q_{il})=\nabla\cdot(\mathbf{K}\nabla Q_{il})+\left[\frac{\partial Q_{il}}{\partial t}\right]_{\text{cond./evap.}}+\left[\frac{\partial Q_{il}}{\partial t}\right]_{\text{coag.}}+\left[\frac{\partial Q_{il}}{\partial t}\right]_{\text{sources/sinks}}, \quad (1)$$

where $\mathbf{u}$ is the wind velocity at the point of interest, $\mathbf{K}$ is the atmospheric eddy diffusivity, $[\partial Q_{il}/\partial t]_{\text{sources/sinks}}$ is the rate of change of aerosol mass of species i in section l due to nucleation, primary aerosol injection and removal, while $[\partial Q_{il}/\partial t]_{\text{cond./evap.}}$ and $[\partial Q_{il}/\partial t]_{\text{coag.}}$

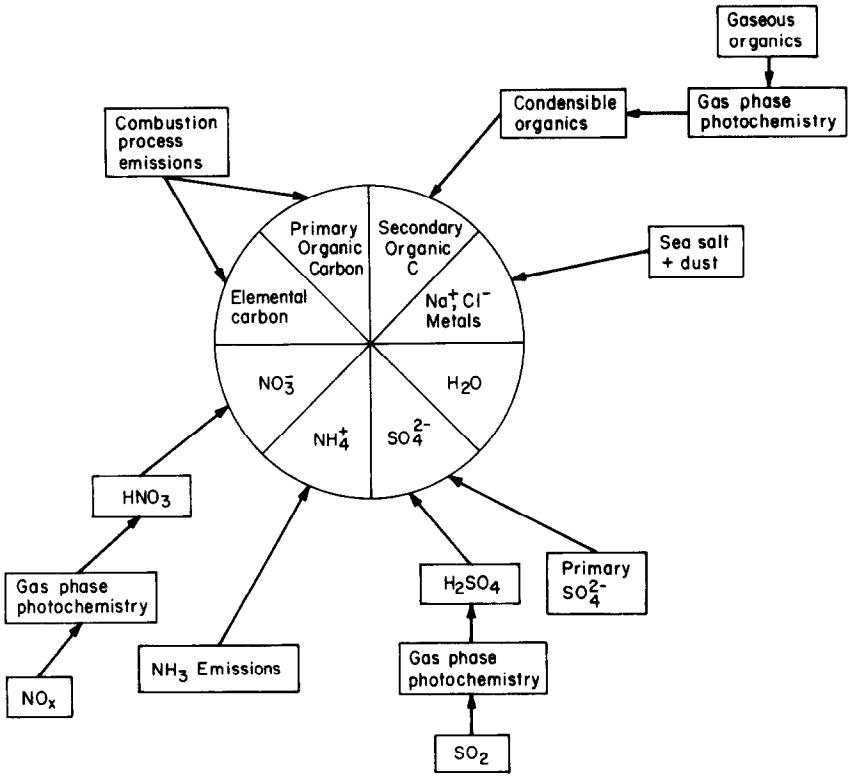

Fig. 1. Idealized schematic of the composition of atmospheric aerosols. The principal sources and particle formation mechanisms are indicated.

are the rates of change due to condensation or evaporation and coagulation, respectively (Gelbard and Seinfeld, 1980; Gelbard *et al.*, 1980; Warren and Seinfeld, 1985; Pilinis *et al.*, 1987).

The evolution of the concentration of the ith gaseous species, C_i is governed by the atmospheric diffusion equation

$$\frac{\partial C_i}{\partial t}+\nabla\cdot(\mathbf{u}C_i)=\nabla\cdot(\mathbf{K}\nabla C_i)+R_i(C_1, C_2, \ldots\ldots, C_n), \tag{2}$$

where R_i is the rate of change of species i via chemical reactions.

Inorganic aerosol constituents

One must account for the rates of transfer of each species between the gas and the aerosol phases. For some species the characteristic time for gas-to-particle transport is sufficiently short that chemical equilibrium is established on a time-scale much shorter than that over which other changes are taking place. This situation is, in fact, estimated to be the case for water, nitric acid and ammonia (Hildemann *et al.*, 1984; Wall *et al.*, 1988; Pilinis and Seinfeld, 1987). Therefore, whereas the gas-to-particle conversion of sulfuric acid and condensable organics is controlled by gas-phase diffusion, the distribution of the volatile inorganic species between the gaseous and particulate phases is calculated using thermodynamic equilibrium.

In the sulfate–nitrate–chloride–sodium–ammonium–water system, the following components are possible:

gas phase: NH_3, HCl, HNO_3, H_2O
liquid phase: H_2O, NH_4^+, SO_4^{2-}, NO_3^-, H^+, Na^+, Cl^-, HSO_4^- and H_2SO_4
solid phase: Na_2SO_4, $NaHSO_4$, NaCl, $NaNO_3$, NH_4Cl, NH_4NO_3, $(NH_4)_2SO_4$, NH_4HSO_4 and $(NH_4)_3H(SO_4)_2$.

Mixed salts of NH_4NO_3 and $(NH_4)_2SO_4$ are not taken into account, because their inclusion is predicted not to affect significantly the distribution of ammonium and nitrate between the gas and the aerosol phases (Saxena *et al.*, 1986). Which of these inorganic species are present at thermodynamic equilibrium depend on the RH and ambient temperature, as well as on the ratio of the $([NH_3]+[NaCl])/[H_2SO_4]$ (Pilinis and Seinfeld, 1987). Because the inorganic portion of the aerosol has been thoroughly addressed by Pilinis and Seinfeld (1987), it will not be discussed further here.

Organic constituents

Organic particulate matter consists of primary and secondary organic compounds. The primary aerosol is the product of combustion processes, while secondary organic aerosol results from condensation of various organic species, the products of gas-phase photooxidation of primary hydrocarbons.

The contribution of the various classes of primary hydrocarbons to the formation of particulate matter depends on their relative ambient concentrations, gas-phase reactivity and ability to form products whose vapor pressure is low enough to produce aerosol.

The oxidation of an atmospheric hydrocarbon HC can be expressed in a general way as (Grosjean, 1977):

$$HC + X \rightarrow I \rightarrow \sum_i a_i P_i,$$

where X is the oxidizing species (e.g. OH and O_3), P_i is the ith product resulting from reactions of the intermediate I, whose formation is the rate-determining step, and a_i is the molar yield.

A sufficiently low vapor pressure for aerosol formation is not thought to occur until the hydrocarbon oxidation products have approximately eight carbon atoms. Since straight-chain olefins of such length exist in the atmosphere only in trace amounts (Grosjean and Fung, 1984) the role of the straight-chain olefins as organic aerosol precursors can be neglected but can be easily added if future work indicates that their aerosol-forming potential is significant.

Cyclic olefins and diolefins have been found to produce aerosol upon photo-oxidation (Hatakeyama *et al.*, 1985, 1987; Izumi *et al.*, 1987). Among the cycloalkenes, cyclopentene and cyclohexene are of major importance, because they are found in gasoline and auto-exhaust. Studies to characterize the chemical identity of the condensable products of the photo-oxidation reactions of these two cycloalkenes have reported that dicarboxylic acids, dialdehydes and oxo-carboxylic acids are the major products in the aerosol phase (Hatakeyama *et al.*, 1985, 1987; Izumi *et al.*, 1987). Dialdehydes are the major primary species produced from the cycloalkene–O_3 reactions, but they are subsequently oxidized to produce oxo-carboxylic acids, the further oxidation of which gives the dicarboxylic acids. The latter species have been reported to be the major aerosol products of the cycloalkene–O_3 reactions (Hatakeyma *et al.*, 1985, 1987). As shown in Table 1, glutaric acid and adipic acid, products of the photo-oxidation of cyclopentene and cyclohexene, respectively, have sufficiently low vapor pressures to form aerosols. Thus, it seems reasonable to assume that these two dicarboxylic acids are the only aerosol products of cyclopentene and cyclohexene and use overall reactions for their production, in the form shown in Table 2.

Product characterization has been attempted by many investigators (O'Brien *et al.*, 1975; Niki *et al.*, 1983) for the reactions of diolefins with O_3. The final

Table 1. Physical properties of condensable organics

Species	Formula	Mol. wt.	D ($m^2 s^{-1}$)	p_0 (Pa)
Succinic acid	$HO_2C(CH_2)_2CO_2H$	118	8.22×10^{-6}	3.96×10^{-5}
Glutaric acid	$HO_2C(CH_2)_3CO_2H$	132	7.51×10^{-6}	1.80×10^{-5}
Adipic acid	$HO_2C(CH_2)_4CO_2H$	146	6.96×10^{-6}	8.19×10^{-6}
Nitro-cresol	$NO_2CH_3C_6H_3OH$	153	7.13×10^{-6}	8.00×10^{-6}

Table 2. Organic aerosol-producing reactions

Reaction	Rate constant ($ppm^{-1} min^{-1}$)	Ref.
$CH_2{=}CH{-}(CH_2)_2{-}CH{=}CH_2 \xrightarrow{O_3} 0.11\ HCOO{-}(CH_2)_2{-}COOH$	8.26×10^{-2}	(a)
$CH_2{=}CH{-}(CH_2)_3{-}CH{=}CH_2 \xrightarrow{O_3} 0.19\ HCOO{-}(CH_2)_3{-}COOH$	5.25×10^{-2}	(a)
$CH_2{=}CH{-}(CH_2)_4{-}CH{=}CH_2 \xrightarrow{O_3} 0.15\ HCOO{-}(CH_2)_4{-}COOH$	3.35×10^{-2}	(a)
Cyclopentene $\xrightarrow{O_3}$ 0.39 $HCOO{-}(CH_2)_3{-}COOH$	1.56	(b)
Cyclohexene $\xrightarrow{O_3}$ 0.15 $HCOO{-}(CH_2)_4{-}COOH$	0.328	(b)
Toluene $\xrightarrow{OH}$ 0.20 cresol	9.10×10^3	(c)
Xylene $\xrightarrow{OH}$ 0.25 cresol	2.65×10^4	(c)
Cresol $\xrightarrow{NO_x}$ 0.30 nitro-cresol	2.20×10^4	(c)

(a) Grosjean (personal communication).
(b) Grosjean and Friedlander (1980); Hatakeyama *et al.* (1987).
(c) Atkinson *et al.* (1982).

products of the diolefin–O_3 reactions are dicarboxylic acids (Schwartz, 1974), which explains the observed high aerosol yields. Three diolefins, 1,5-hexadiene, 1,6-heptadiene and 1,7-octadiene, are included in the primary organic inventory of aerosol precursors. The overall reactions of the diolefins are shown in Table 2, and the physical properties of their condensable products are summarized in Table 1.

Another class of organics that gives aerosol products, upon atmospheric photo-oxidation, is aromatics. Aromatics currently comprise about 35% of the gasoline in the United States and are also used as industrial solvents. Among the various aromatics, toluene and the xylenes are of major importance, because they are present in substantial levels in urban air (Grosjean and Fung, 1984).

In spite of numerous experimental studies, the detailed reaction pathways of aromatic photo-oxidations are still not well understood (Atkinson *et al.*, 1980; Leone and Seinfeld, 1984; Gery *et al.*, 1985, 1987). Rate constant considerations indicate that aromatics will react predominantly with OH. Three reactions involving aromatic hydrocarbons are included in the current organic aerosol mechanism. Because of similarities in their reaction mechanisms and rate constants, *o*-,*p*-,*m*-xylenes are lumped together. The major products of the toluene–OH and xylene–OH reactions are cresols and dimethyl phenols. The molar yield of the cresol production from the first reaction is estimated to be about 20% of the reacted toluene, while the yield of the latter reaction is estimated to be about 25% of the reacted xylene (Atkinson and Lloyd, 1984; Gery *et al.*, 1985, 1987). Once cresols and dimethylphenols are formed, various nitrocresol and nitroxylene products result through addition of radicals (Gery *et al.*, 1985, 1987). It is estimated that the yield of the nitro-cresol formation is about 30% of the cresols and of the phenols reacted.

Physical properties of the various condensable species produced by the aromatic hydrocarbons photo-oxidation reactions are not generally known. For the purpose of our calculations the diffusion coefficient, molecular weight and solubility of all aromatic aerosol organics were assumed to be those of nitro-cresol, while saturation vapor pressure data for the condensable species were taken from recent smog chamber experiments (Seinfeld *et al.*, 1987) and are listed in Table 1.

Gas-phase chemistry

The chemical mechanism used in this model is that previously employed by Russell *et al.* (1988). Estimated emission rates of various hydrocarbons in the South Coast Air Basin of California in 1982 are listed in Table 3. Based on these estimated emission rates, cyclopentene, toluene and xylene are assumed to be the only organic aerosol precursors, from the ones discussed previously, present in the South Coast Air Basin. The potential exists in the model, however, to include the emissions of other organic precursors once their emission rates have been estimated. Because gridded hydrocarbon emissions and ambient concentrations are not generally speciated into the organic compounds needed by chemical mechanisms, splitting factors must be used so that the specific organic species emissions or concentrations can be determined as the product of the species splitting factor and the total emission rate or concentration of organics. Using the estimates of Table 3 and results of previous work (Gray *et al.*, 1986; Russell *et al.*, 1988), a set of splitting factors for the non-methane organic species involved in the chemical reaction mechanism, including the organic aerosol precursors, has been developed and is listed in Table 4.

Table 3. Estimated organic emission rates in the South Coast Air Basin of CA*

Species	Emissions (ton day^{-1})
Methane	1202.8
Toluene	105.5
Pentane	89.6
Butane	66.7
Ethane	59.7
Ethylene	55.3
Octane	49.4
Xylene	43.9
Heptane	49.9
Propylene	36.8
Chloroethylene	33.2
Acetylene	32.7
Hexane	31.1
Propane	26.2
Benzene	19.0
1,1,1-Trichloroethane	16.1
Pentene	13.2
N-Butyl acetate	13.1
Acetone	12.9
N-Pentadecane	12.4
Cyclohexane	12.4
Methyl-ethyl ketone	11.1
Acetaldehyde	10.6
Trimethylbenzene	10.0
Ethylbenzene	8.4
Methyl-ethyl ketone	11.1
Naphtha	8.0
Methyl-cyclohexane	7.5
Nonane	5.8
Methyl alcohol	5.6
1-Hexene	5.4
Methyl-cyclopentane	5.0
Methyl-pentane	4.8
Dimethyl-hexane	4.6
Cyclopentene	0.4

*Source: South Coast Air Quality Management District.

Computational implementation

The region, for which the air quality is to be simulated, is part of the South Coast Air Basin of California (Fig. 2). In the vertical direction the calculation is extended up to 1100 m above ground level. It has been shown in previous work (Russell *et al.*, 1988) that five vertical layers, unequally distributed, provide

Table 4. Hydrocarbon splitting factors*

Species†	Urban	Rural	Ocean
HCHO	3.7×10^{-3}	1.0×10^{-3}	1.0×10^{-3}
RCHO	3.3×10^{-3}	2.0×10^{-3}	5.0×10^{-3}
Ole	4.2×10^{-3}	6.0×10^{-4}	1.0×10^{-4}
Alk	6.8×10^{-2}	2.3×10^{-2}	9.6×10^{-3}
C_2H_4	6.1×10^{-3}	4.0×10^{-3}	6.0×10^{-3}
Toluene‡	1.1×10^{-2}	3.3×10^{-3}	1.1×10^{-3}
Xylene‡	3.9×10^{-3}	1.2×10^{-3}	3.8×10^{-4}
Prim. org. aer.§	7.0×10^{-3}	7.0×10^{-3}	7.0×10^{-3}
Cyclopentene‖	7.0×10^{-5}	1.0×10^{-5}	1.7×10^{-6}

* When multiplied by the total organic concentrations, these splitting factors produce the individual species concentrations.

† These are the organic species in the chemical reaction mechanism of Russell *et al.* (1988) appended with the primary organic aerosol and the organic aerosol precursors, toluene, xylene and cyclopentene.

‡ Based on Table 3, toluene and xylene emission rates are estimated to be about 63.4% and 22.3% of the total aromatic emissions, respectively. These values, when multiplied by the splitting factors for aromatics used by Russell *et al.* (1988), give the toluene and xylene splitting factors.

§ These splitting factors have been derived so that, when multiplied by the initial total hydrocarbon concentrations, they give initial primary organic concentrations close to those observed in various sites in the South Coast Air Basin of California on 27 August 1982. The emissions of primary organics are correlated with the total hydrocarbon emissions. A factor 0.21 has been found, when multiplied with the total aromatic emissions, to give about 40 ton day^{-1} of primary organic aerosol emissions, consistent with recent estimates of primary organic aerosol emissions over the Los Angeles area (Gray *et al.*, 1986).

‖ These factors have been derived from measurements taken by Grosjean and Fung (1984) of the speciated hydrocarbon composition in Los Angeles and the splitting factors of OLE used by Russell *et al.* (1988).

a good compromise between computing time requirements and acceptable representation of the vertical variation of the predicted concentrations of the various major gas-phase pollutants. Each horizontal layer consists of 681 cells, as shown in Fig. 2, with dimensions 5 km × 5 km. Hence, 3405 cells are involved in the implementation of the model for this region.

The set of Equations (1) and (2) is solved using an operator splitting technique, in order to decouple the horizontal transport, the vertical transport, the gas-phase chemistry and the aerosol growth and coagulation (McRae *et al.*, 1982b). The operator scheme used here to calculate the value of the variable vector F_i at time $t+2h$ is

$$F_i^{(t+2h)} = A_x(h)A_y(h)A_{zc}(2h)A_y(h)A_x(h)F_i^{(t)} \quad (3)$$

for the non-condensable gases, while

$$F_i^{(t+2h)} = A_i(2h)A_{th}(2h)A_d(2h)A_x(h)A_y(h) \times A_{zc}(2h)A_y(h)A_x(h)F_i^{(t)} \quad (4)$$

for the aerosol species and the condensable gases. A_x, A_y, A_{zc} are the x-transport, y-transport, z-transport and gas-phase chemistry operators, respectively, while A_i, A_{th}, A_d are the operators for the intersectional movement of the aerosol particles, the aerosol thermodynamics and the aerosol dynamics, respectively.

The structure of the entire model is shown in Fig. 3. For the advection part of A_x and A_y a linear finite element scheme with Crank–Nicholson time differencing and a noise filter is applied, while a finite difference scheme is used for the diffusion term of these operators (McRae *et al.*, 1982b). In the A_{zc} operator, a

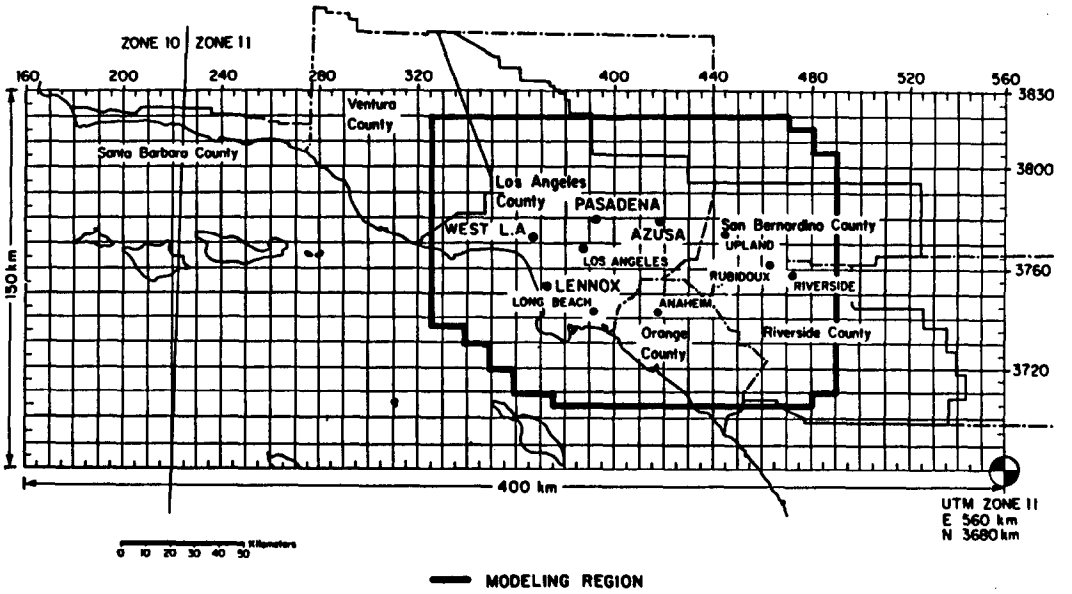

Fig. 2. The South Coast Air Basin of California. Emissions and meteorological data fields are developed over the 400 km × 150 km gridded area. Air quality modeling calculations are performed within the region bounded by the heavy solid line.

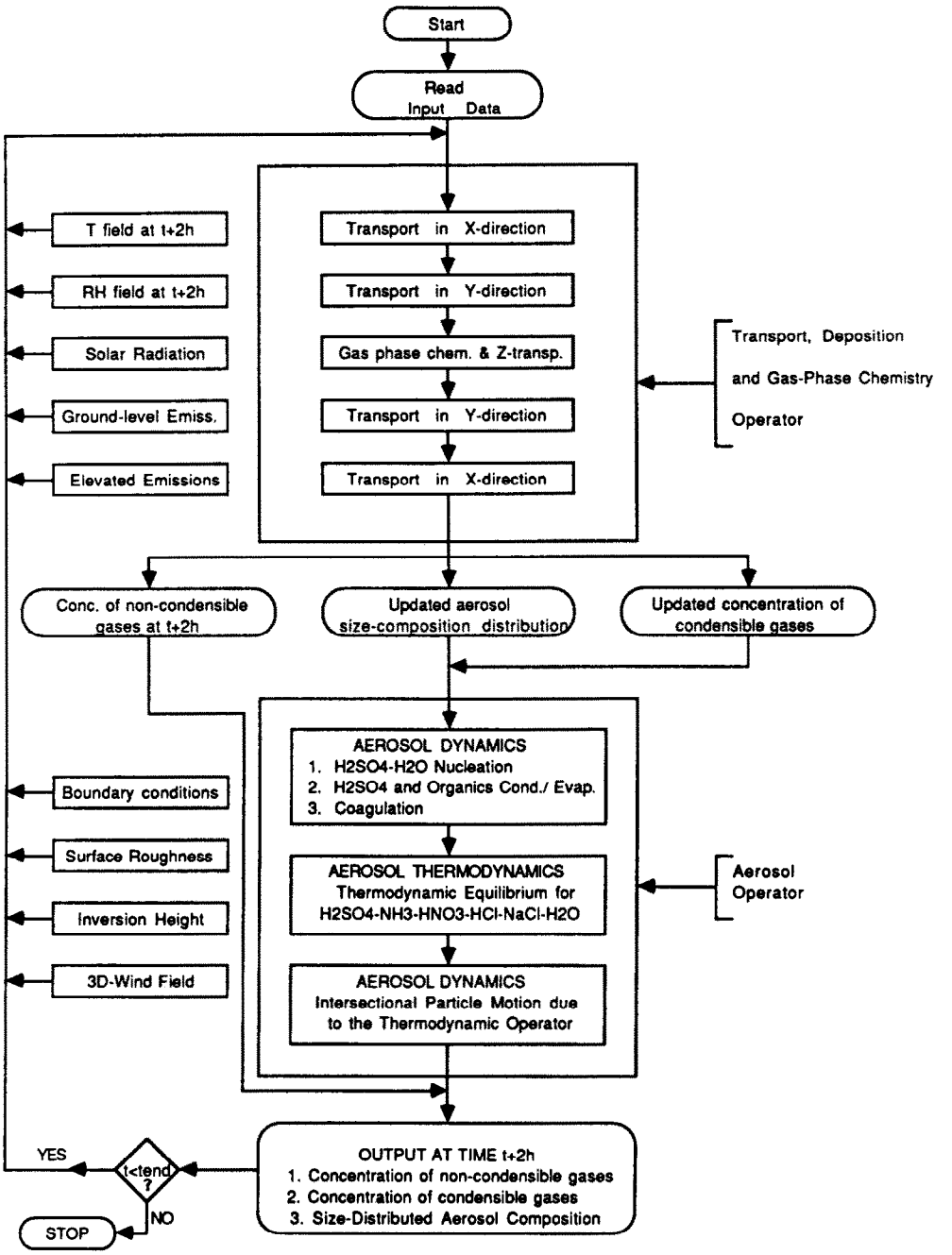

Fig. 3. Schematic representation of the structure of the numerical model.

simple explicit finite difference scheme is used for the transport, while a predictor-evaluation-corrector method is used for the gas-phase chemistry, which involves 33 gas-phase species (Russell *et al.*, 1988). Thus, with 3405 cells in the modeling region, 112,365 ordinary differential equations have to be solved at each time-step, for the gas-phase chemistry.

The aerosol operator A_d deals with the condensation of sulfuric acid and the four condensable organics of Table 1, the generation of new aerosol by homogeneous heteromolecular nucleation of H_2SO_4–H_2O, introduction of primary particles, such as sodium and primary carbon, as well as coagulation and intersectional motion of both volatile and non-volatile species (Pilinis *et al.*, 1987). One ordinary differential equation is required for each species in each section to describe its evolution from the above processes. Thus, for each computational cell of the modeling region [8 × (number of aerosol sections) + 5] ordinary differential equations have to be solved. For 3405 cells, with the aerosol assumed to consist of three sections, two fine and one coarse, 98,745 ordinary differential equa-

tions result, which are solved with EPISODE O.D.E. solver routine (Hindmarsh and Byrne, 1975).

A_{th} represents the equilibrium calculation. For each cell it is necessary to determine the equilibrium concentrations for the HNO_3–NH_3–H_2SO_4–NaCl–HCl–H_2O system, which involves 18 aerosol and three gaseous species. This equilibrium calculation involves $[3405 \times (18 \times 3 + 3)]$ algebraic equations that have to be solved at each time-step (Pilinis and Seinfeld, 1987). Finally, the A_i operator deals with the intersectional migration of the various species due to the condensation of the volatile components (Pilinis *et al.*, 1987). Depending on the thermodynamically possible species predicted in the equilibrium calculation, in which up to 22 species are involved, this part may require the solution of as many as $3405 \times 3 \times 22 = 224{,}730$ ordinary differential equations. Output at the end of each time-step is the new size-distributed aerosol chemical composition and the concentrations of the gas-phase species. All the species predicted by the model are listed in Table 5.

INPUT DATA FOR THE MODEL

Input data include the region definition and its topography and surface roughness distribution, three-dimensional wind fields, spatial and temporal temperature and RH profiles, solar radiation and cloud cover, surface and elevated area and point source emissions, as well as initial and boundary gas-phase concentrations and aerosol size–composition distributions. The input data used in this calculation are listed in Table 6.

Because of the lack of any information about the size distributions of sulfate, sodium and organics throughout the South Coast Air Basin at 0000 PST (Pacific Standard Time) on the simulation day of 30 August 1982, default initial size distributions, based on observations in the Los Angeles area (Wolff and Klimisch, 1982; Wall *et al.*, 1988), are used. From a computational point of view, the aerosol is assumed to consist of three size sections, two fine and one coarse, with ranges 0.05–0.3, 0.3–2.0 and 2.0–10.0 μm. Given these sections, the initial concentrations of HNO_3, NH_3, H_2SO_4, HCl and NaCl, and the initial temperature and RH fields, the size-distributed composition and physical state of the aerosol at 0000 PST are predicted throughout the region of interest by the chemical equilibrium calculation, while the initial aerosol organic concentrations are calculated, using the splitting factors of Table 4.

Table 5. Variables predicted by the model

Gas phase
CO, O_3, NO, NO_2, PAN,
HNO_3, NH_3, H_2SO_4, SO_2,
toluene, xylene, cyclopentene,
nitrocresol, cyclohexene, cresol,
C_6H_{10}, C_7H_{12}, C_8H_{14},
$C_4H_6O_4$, $C_5H_8O_4$, $C_6H_{10}O_4$

Aerosol phase
1. Size-distributed
   H_2O, NH_4^+, SO_4^{2-}, NO_3^-, H^+,
   Na^+, Cl^-, HSO_4^-, H_2SO_4,
   Na_2SO_4, $NaHSO_4$, NaCl, $NaNO_3$, NH_4Cl,
   NH_4NO_3, $(NH_4)_2SO_4$, NH_4HSO_4,
   $(NH_4)_3H(SO_4)_2$,
   primary and secondary organics
2. Total concentration
   Sulfate
   Nitrate
   Chloride
   Sodium
   Ammonium
   Water
   Primary and secondary organics
3. Total volatiles
4. Total aerosol mass

APPLICATION OF THE MODEL TO THE SOUTH COAST AIR BASIN ON 30 AUGUST 1982

The Eulerian gas–aerosol model, using the initial conditions and emission inventories described above, has been applied to the South Coast Air Basin of California from 0000 to 2400 PST on 30 August 1982, for which 4-h average concentration data for sulfate, nitrate, ammonium, chloride, sodium, calcium and magnesium are available. Whenever Ca and Mg are present, their concentrations were reduced to equivalent Na in order to be included in the equilibrium calculation. About 8 CPU h on the San Diego Supercomputer Center CRAY X-MP were required for the 24-h simulation.

Figures 4 and 5 show the predicted concentrations of sulfate, nitrate, ammonium, sodium and chloride at Long Beach and Rubidoux, CA. These figures also show the evolution of the water, total aerosol concentrations, and various organic species over the course of the day.

The predictions are seen to exhibit the same behaviour as the observed aerosol species concentrations, generally within the uncertainty of the measurements. The predicted chloride concentrations at Rubidoux are much higher than those observed. This discrepancy could be attributable to our assumption concerning the total chloride concentration. Despite the fact that 4-h averaged aerosol chloride measurements were available, no gaseous HCl measurements were available. In the absence of HCl data it was assumed that the total airborne chloride concentration was equal to that for sodium. This assumption is no doubt more adequate for the coastal sites, where fresh NaCl flows inland, than inland, at locations like Rubidoux, where the total chlorides are overestimated, since the coastal NaCl reacts with H_2SO_4 and HNO_3 to produce more stable compounds than NaCl before it reaches those areas (Harrison and Pio, 1983). Predicted nitrate and ammonium concentrations vary from low values at the coastal sites to high values inland, consistent with the observed behavior.

Table 6. Input data to the model for 30 August 1982

Parameter	Source of measured data	Method of derivation of gridded-data
3-D wind fields	SCAQMD,* CARB,† NWS‡	Interpolation over the 80 × 30 grid of Fig. 2
Solar radiation	JPL,§ CARB, SCAQMD	
Cloud cover	JPL, CARB, SCAQMD	
Inversion height		Russell *et al.* (1987)
Emission inventory of gaseous pollutants (except of NH_3)		CARB, SoCAB 1982 forecast emission inventory
NH_3 emission inventory		Cass and Gharib (1984)
Ionic species (Ca and Mg) emissions (in equivalent Na)‖		2.0×10^{-4} ppm m min^{-1}
RH and T	SCAQMD, CARB, NWS	Interpolation over the 80 × 30 grid of Fig. 2
Ground-level initial conditions (0000 PST)	SCAQMD for gases Hildemann *et al.* (1984) for aerosol species	Interpolation over the 80 × 30 grid of Fig. 2
Upper-level initial conditions		Interpolation between the ground-level initial conditions and background concentrations¶
Initial concentrations of condensible organics		Set equal to zero
Boundary conditions		Set to the concentrations of the various gas and aerosol species at the edge of the small region of Fig. 2; they are defined by the values of the interpolated conc. over the 80 × 30 grid, at the edge of the modeling region

* SCAQMD, South Coast Air Quality Management District.
† CARB, California Air Resources Board.
‡ NWS, National Weather Service.
§ JPL, Jet Propulsion Laboratory.
‖ Major sources of Ca and Mg on 30 August 1982 were soil dust particles emitted during construction and other anthropogenic activities (Cass, personal communication). Due to the lack of any data regarding dust emissions, the value of 2.0 $\times 10^{-4}$ ppm m min^{-1}, based on the maximum average concentration increase observed during that day (Hildemann *et al.*, 1984), is used for these species.
¶ Background concentrations of various gases are given by Russel *et al.* (1988). Background concentrations of organic aerosol precursors are calculated from the corresponding total background hydrocarbon concentrations using the splitting factors of Table 4, while those of sulfate and sodium chloride are set at 0.5 ppb.

As shown in Figs 4(f)–5(f), the total aerosol concentration follows the amount of water in the aerosol phase. Early in the morning, because of high RHs, water is predicted to account for about 50% of the total aerosol mass. During the day, increasing temperature and decreasing RH cause water to evaporate, thus reducing the total aerosol concentration, which is predicted to reach a minimum around 1600 PST at most of the sites. Later in the evening, because of increasing RH, a second peak in the water concentration is predicted to cause a rapid increase in the total aerosol concentration. High temperatures during the day also cause the evaporation of the other volatile species, especially chloride, the concentration of which is predicted to reach a minimum between 1200 and 1600 PST.

Figures 4(g)–5(g) show the evolution of the secondary and total organic concentrations at Long Beach and Rubidoux, respectively. As shown in these figures, most of the aerosol organics are predicted to be primary organic species. The secondary organic concentrations at Rubidoux are predicted to be higher than those at Long Beach, primarily because Rubidoux is a receptor of the products of photochemical activity. Most of the secondary organics are predicted to be nitro-cresols, products of toluene and xylene photochemical reactions. Both at Long Beach and Rubidoux the primary organic concentrations reach a maximum at about 1200 PST. Later in the day, though, the rising mixing depth leads to dilution.

Figures 6 and 7 show the predicted size–composition distributions at 0000, 1200 and 2400 PST at Long Beach and Rubidoux. A common characteristic of these size distributions is that early in the morning, when RH $\geqslant$ 75%, sufficient water is predicted to exist in the aerosol phase to dissolve the ionic species. From 900 PST to 1800 PST the RH falls below the deliquescence point of all the thermodynamically possible salts (Pilinis *et al.*, 1987), resulting in dry particles. Predominant compounds in the aerosol phase during this period are predicted to be Na_2SO_4, $(NH_4)_2SO_4$, $NaNO_3$ and NH_4NO_3. A substantial quantity of nitrate is predicted to be associated with the existence of sodium in the coarse particles, providing an explanation of why the median diameter for nitrates is generally observed to be larger than that of the sulfates (Hidy *et al.*, 1975; Harrison and Pio, 1983; Wall *et al.*, 1988).

After 1800 PST the ambient RH again starts increasing, leading to the gradual dissolution of the various ionic species and the growth of the particles. At the end of the day, when the RH is above 80%, most of the aerosol mass is predicted to lie in the coarse section, with water accounting for more than

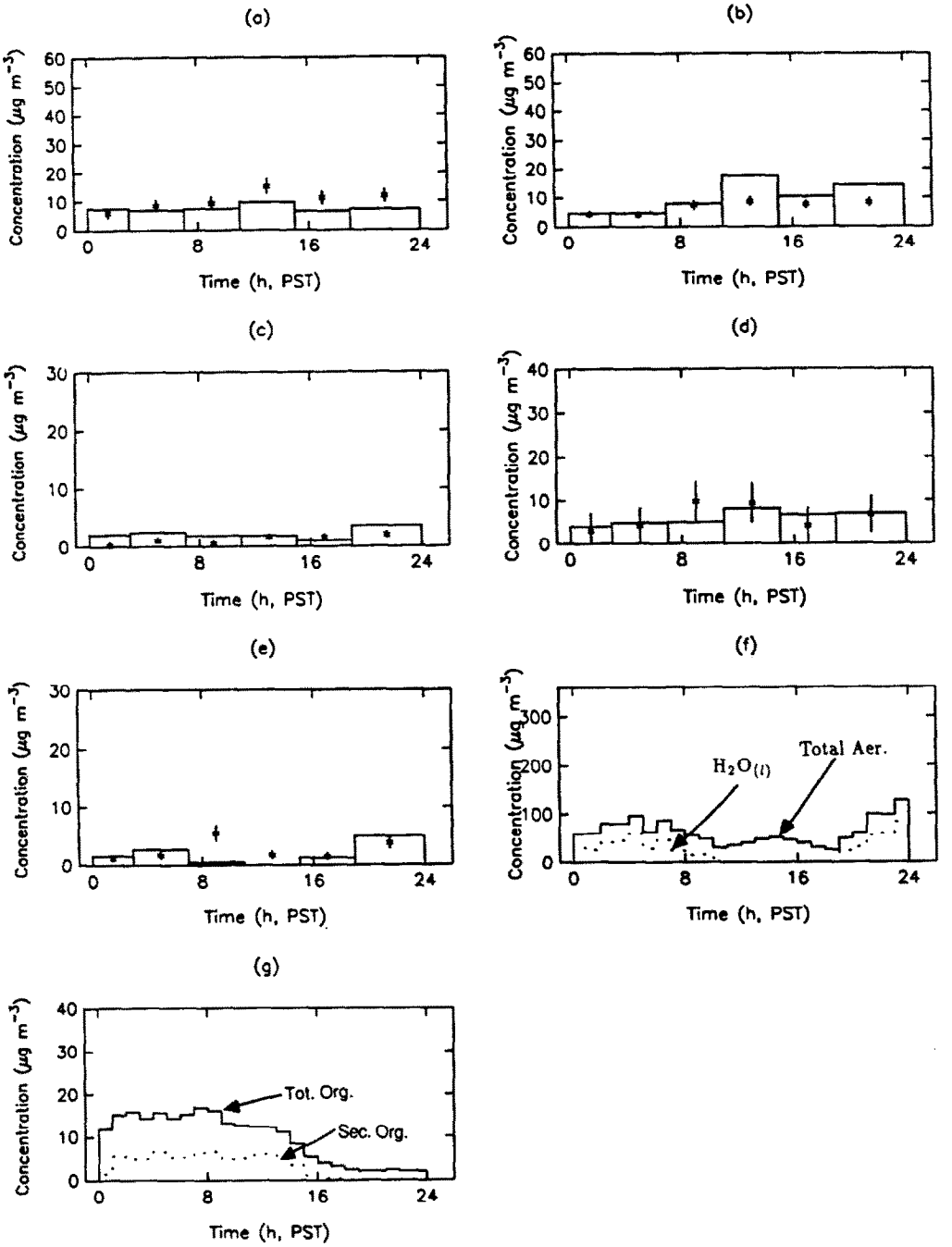

Fig. 4. Predicted and observed concentrations of (a) sulfate, (b) nitrate, (c) ammonium, (d) equivalent sodium and (e) chloride, as well as predicted concentrations of (f) aerosol water and total aerosol, (g) secondary and total organic aerosol at Long Beach, CA, on 30 August 1982.

50% of the aerosol mass, consistent with various observations in Los Angeles (Ho *et al.*, 1974).

STATISTICAL EVALUATION OF MODEL PERFORMANCE

A statistical analysis of the deviation between model predictions and observations is a key element of model performance evaluation. Many statistical tests may be used to evaluate the performance of air quality models (Bencala and Seinfeld, 1979; Rao *et al.*, 1985; Ku *et al.*, 1987; Russell *et al.*, 1988).

Table 7 contains a number of performance measures, their defining equations, and their values for the 30 August 1982 simulation. The mean of the residuals is positive for the sulfate and sodium, indicating underprediction, whereas it is negative for nitrates,

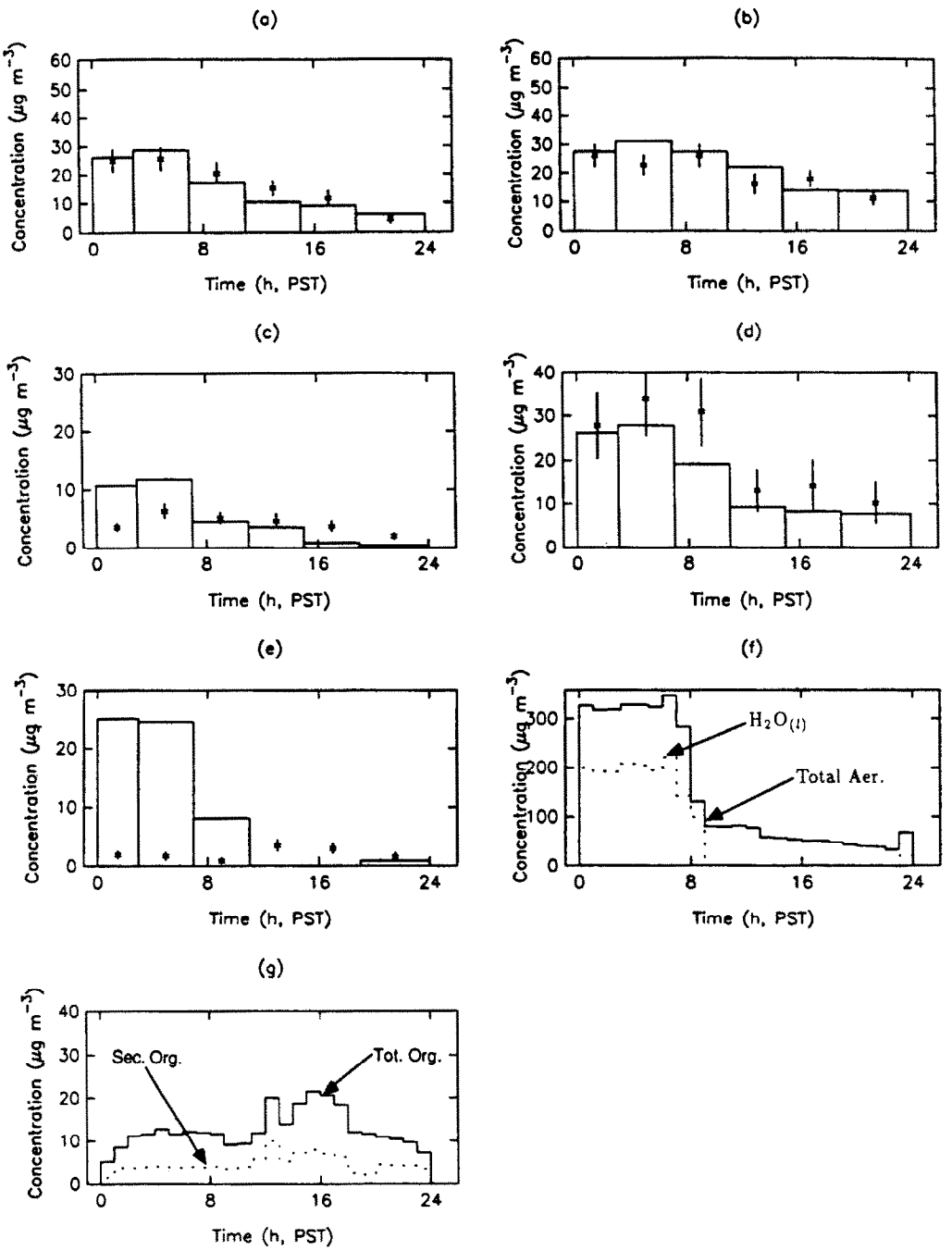

Fig. 5. Predicted and observed concentrations of (a) sulfate, (b) nitrate, (c) ammonium, (d) equivalent sodium and (e) chloride, as well as predicted concentrations of (f) aerosol water and total aerosol, (g) secondary and total organic aerosol at Rubidoux, CA, on 30 August 1982.

ammonium and chlorides, indicating overprediction of the model with respect to those species.

We have also computed the correlation coefficient between observations and predictions, as well as the index of the agreement. The correlation coefficient, in general, shows the extent to which the predicted concentrations increase linearly with the observed ones. The index of agreement is a stricter test, because it is sensitive to differences between the measured and predicted means, as well as to changes in proportionality. Both of these statistical criteria show agreement between observations and predictions for all the species, except the chlorides. The performance for chlorides was poor, of the order of 0.2, for both the correlation coefficient and the index of agreement. This discrepancy may be a result of the assumed initial total chloride concentrations inland. This possibility is supported by the fact that, if the predicted chloride

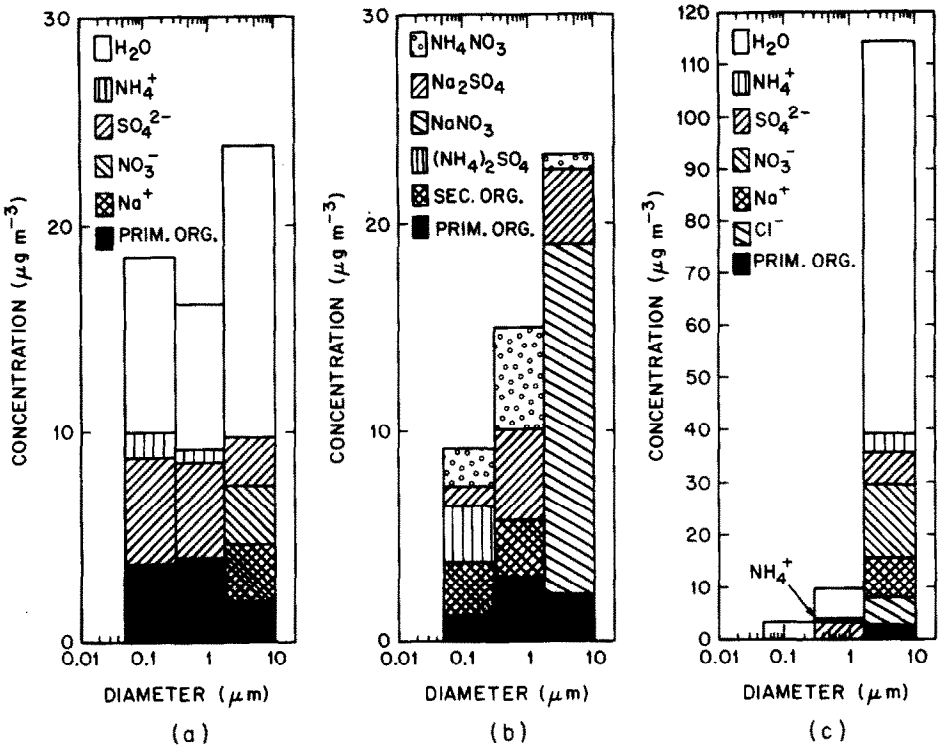

Fig. 6. Predicted aerosol size–composition distribution at Long Beach, CA, at (a) 0200 PST, (b) 1200 PST and (c) 2400 PST on 30 August 1982. The mass below the upper line indicates the total amount of aerosol, with the incremental components of that total indicated.

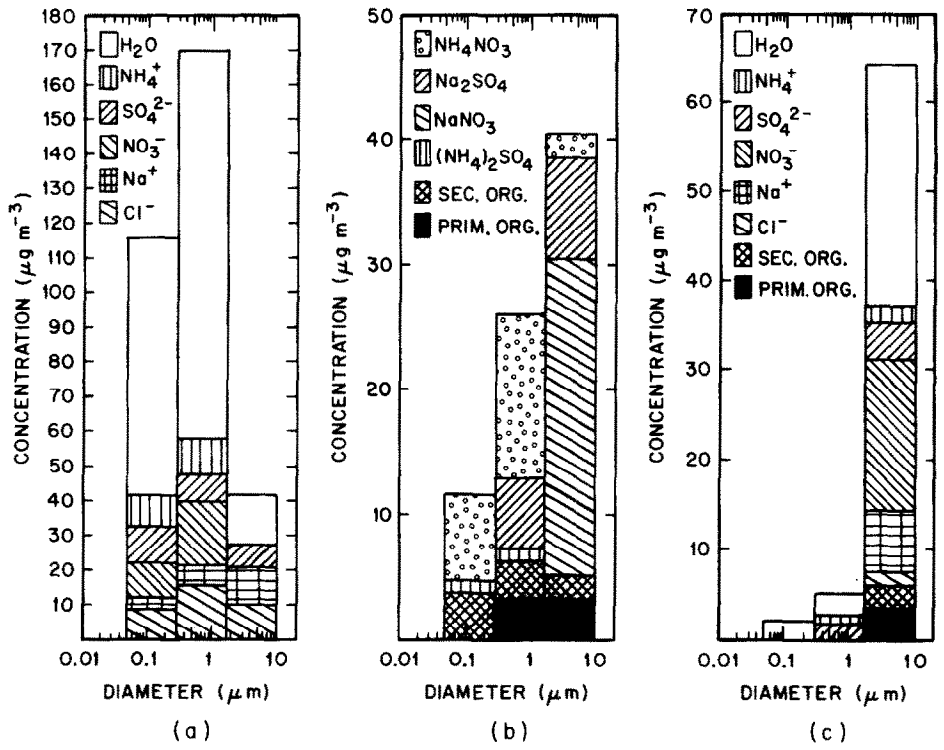

Fig. 7. Predicted size–composition distribution at Rubidoux, CA, at (a) 0000 PST, (b) 1200 PST and (c) 2400 PST on 30 August 1982. The mass below the upper line indicates the total amount of aerosol, with the incremental components of that total indicated.

Table 7. Statistical evaluation of model performance for various ionic aerosol species

Performance measure	Definition	Species				
		SO_4^{2-}	NO_3^-	NH_4^+	Na^+	Cl^-
Mean observed ($\mu g\,m^{-3}$)	$\mu_0 = \frac{1}{n}\sum_{i=1}^{n} O_i$	10.54	8.91	2.11	6.89	1.36
SD observed ($\mu g\,m^{-3}$)	$s_0 = \left[\frac{1}{n-1}\sum_{i=1}^{n}(O_i-\mu_0)^2\right]^{1/2}$	6.10	6.64	1.75	6.63	1.47
Mean predicted ($\mu g\,m^{-3}$)	$\mu_p = \frac{1}{n}\sum_{i=1}^{n} P_i$	8.74	13.36	3.39	6.67	2.61
SD predicted ($\mu g\,m^{-3}$)	$s_p = \left[\frac{1}{n-1}\sum_{i=1}^{n}(P_i-\mu_p)^2\right]^{1/2}$	5.59	9.54	3.31	4.86	4.79
Mean of residuals ($\mu g\,m^{-3}$)	$\mu_R = \frac{1}{n}\sum_{i=1}^{n}(O_i-p_i)$	1.80	−4.44	−1.28	0.23	−1.25
Slope	$m = \frac{\sum_{i=1}^{n} O_i P_i - \frac{1}{n}\sum_{i=1}^{n} O_i \sum_{i=1}^{n} P_i}{\sum_{i=1}^{n} O_i^2 - \frac{1}{n}\left(\sum_{i=1}^{n} O_i\right)^2}$	0.602	0.920	1.226	0.635	0.631

Intercept ($\mu g\,m^{-3}$)	$b=\frac{1}{n}\left(\sum_{i=1}^{n}P_i-m\sum_{i=1}^{n}O_i\right)$	2.391	5.163	0.809	2.293	1.753
Correlation coefficient	$\rho=\frac{ms_0}{s_p}$	0.66	0.64	0.65	0.86	0.20
Average absolute gross error ($\mu g\,m^{-3}$)	$A=\frac{1}{n}\sum_{i=1}^{n}\lvert O_i-P_i\rvert$	3.63	5.65	1.90	2.36	2.17
Index of agreement	$I=1-\frac{\sum_{i=1}^{n}(O_i-P_i)^2}{\sum_{i=1}^{n}(\lvert P_i-\mu_0\rvert+\lvert O_i-\mu_0\rvert)^2}$	0.79	0.71	0.67	0.90	0.23
R.M.S.E. ($\mu g\,m^{-3}$)	$\sigma=\left[\frac{1}{n}\sum_{i=1}^{n}(O_i-P_i-\mu_R)^2\right]^{1/2}$	4.82	7.29	2.53	3.40	4.69
M.S.E.$_u$ ($\mu g\,m^{-3}$)^2	$\text{M.S.E.}_u=\frac{1}{n}\sum_{i=1}^{n}(mO_i+b-P_i)^2$	17.48	52.89	6.23	5.91	21.74
M.S.E.$_s$ ($\mu g\,m^{-3}$)^2	$\text{M.S.E.}_s=\frac{1}{n}\sum_{i=1}^{n}(mO_i+b-O_i)^2$	9.05	20.02	1.81	5.70	1.85
M.S.E.$_u$/M.S.E	%	65.9	72.5	77.5	50.9	92.1
M.S.E.$_s$/M.S.E	%	34.1	27.5	22.5	49.1	7.9

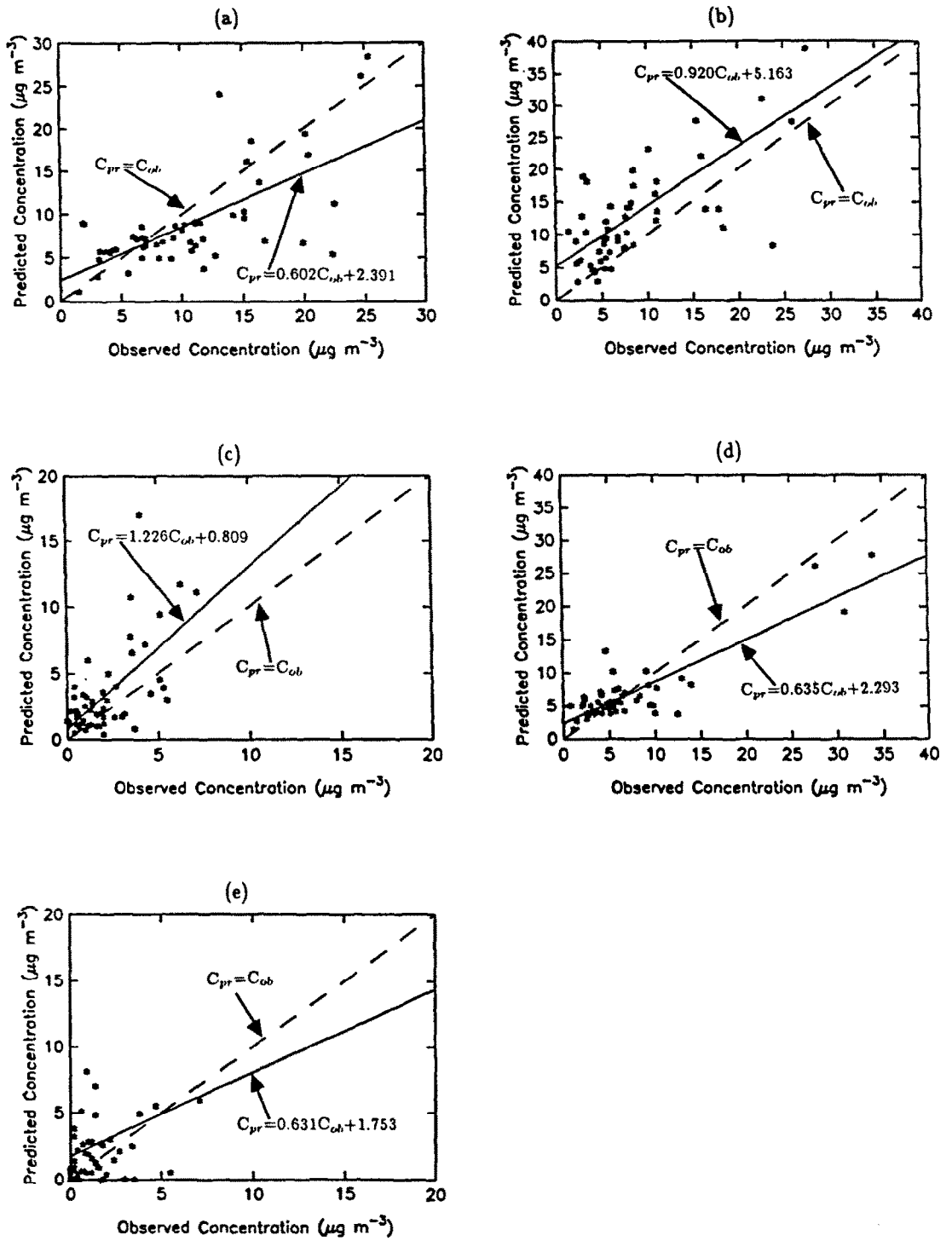

Fig. 8. Linear least squares lines for predicted and observed concentrations of (a) sulfate, (b) nitrate, (c) ammonium, (d) equivalent sodium and (e) chloride determined over all times and locations of the 24-h application of the model in the SoCAB on 30 August 1982.

concentrations at Upland and Rubidoux are not included, the correlation coefficient increases from 0.2 to 0.5, while the index of agreement increases from 0.23 to 0.7.

Figure 8 shows the linear least squares lines for all the ionic species. Perfect agreement would have all points falling on the 45° line. The predicted lines are within 15° of the 45° line. Residual frequency plots (Fig. 9) show that the residual differences between the predicted and observed concentrations for all the ionic aerosol species.

The last test performed and listed in Table 7 is the mean-square error (M.S.E.), which consists of the systematic(s) and unsystematic(u) parts. These statisti-

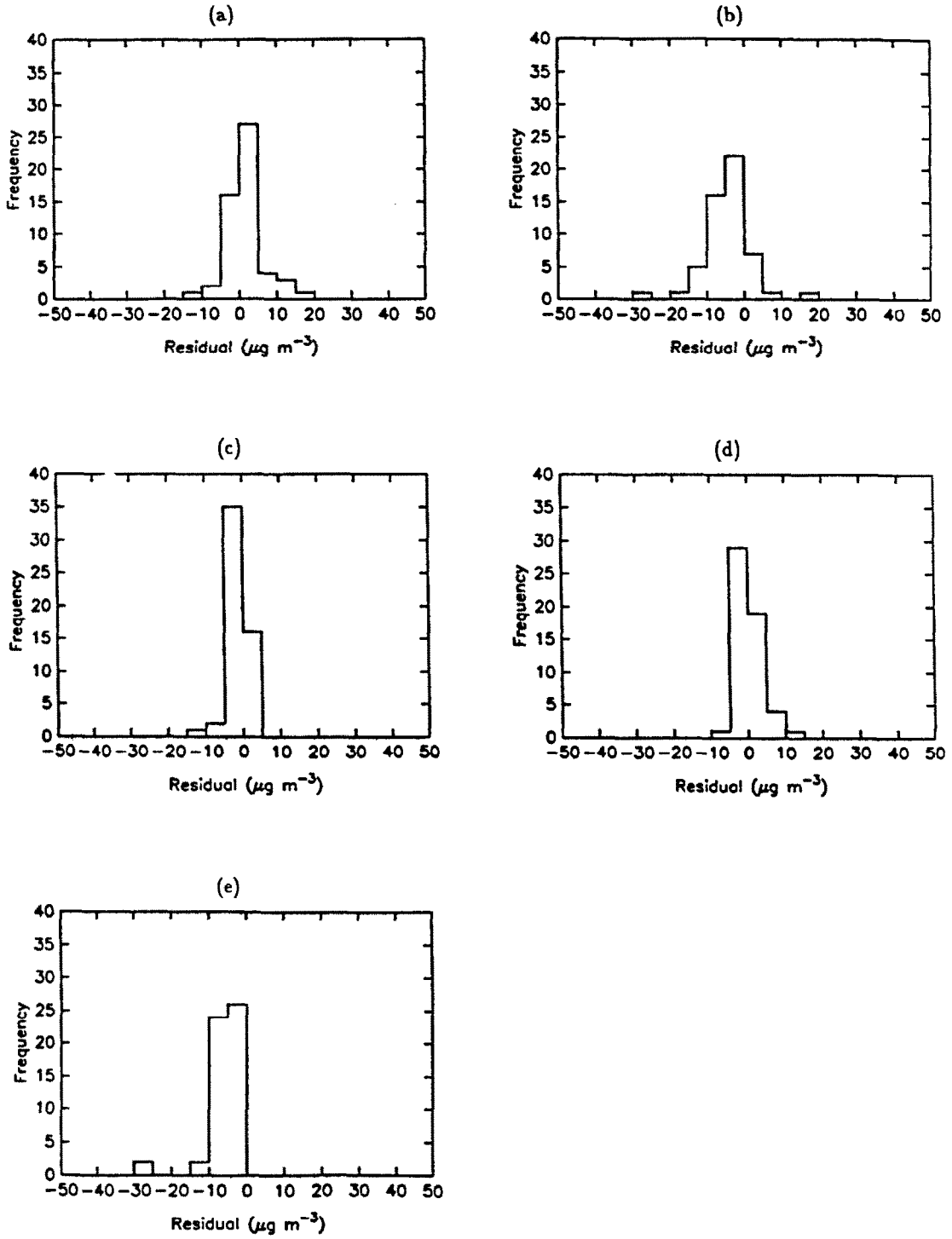

Fig. 9. Histograms of concentration residuals (observed minus predicted) for (a) sulfate, (b) nitrate, (c) ammonium, (d) equivalent sodium and (e) chloride determined over all times and locations of the 24-h application of the model in the SoCAB on 30 August 1982.

cal measures can be used to indicate the extent to which a model may be improved (Rao *et al.*, 1985; Ku *et al.*, 1987). The contribution of the M.S.E.$_u$ to the mean-square error is seen in the present case to be more important than that of the M.S.E.$_s$, which means that improvements in the model may not be as possible as if systematic errors were present.

CONCLUSIONS

An urban multicomponent Eulerian aerosol model has been developed by coupling a model that predicts the size–composition distribution of atmospheric aerosols to a grid-based, gas-phase urban airshed model. Model performance was evaluated by com-

parison against measured aerosol concentrations on 30 August 1982, in the South Coast Air Basin of California. The model has provided the first three-dimensional predictions of the concentrations and size distribution of inorganic and organic aerosol species over an urban airshed.

The inorganic aerosol phase was predicted to consist of an aqueous solution of various inorganic species during the early hours of the day and late at night, during which the RH was high, and of a solid phase during the rest of the day, when the RH was low. Water is predicted to play an important role in shaping the aerosol size distribution. Besides the fact that water is predicted to account for more than 50% of the aerosol mass at humidities above 80%, its condensation causes the growth of the particles into the coarse-particle regime.

Volatile aerosol constituents are predicted to be quite sensitive to temperature changes. Sulfate and nitrate were predicted to be the major inorganic aerosol species, whose hygroscopicity causes the water condensation, while primary organics were the major organic species in the aerosol phase.

Acknowledgements—This work was supported by the State of California Air Resources Board Agreement A732-043. Computing time was provided by a grant from the San Diego Supercomputer Center.

REFERENCES

Atkinson R., Carter W. P. L., Darnall R., Winer A. M. and Pitts J. N. (1980) A smog chamber and modeling study of the gas phase NO_x–air photooxidation of toluene and cresols. *Int. J. chem. Kinet.* **12,** 779.

Atkinson R. and Lloyd A. C. (1984) Evaluation of kinetic and mechanistic data for modelling of photochemical smog. *J. Phys. Chem. Ref. Data* **13,** 315.

Atkinson R. and Lloyd A. C. and Winges L. (1982) An updated chemical mechanism for hydrocarbon/NO_x/SO_2 photooxidations suitable for inclusion in atmospheric simulation models. *Atmospheric Environment* **16,** 1341–1355.

Bencala K. E. and Seinfeld J. H. (1979) An air quality model performance assessment package. *Atmospheric Environment* **13,** 1181–1185.

Cass G. R. and Gharib S. (1984) Ammonia emissions in the South Coast Air Basin 1982. Open File Rep. 84-2, Environmental Quality Laboratory, California Institute of Technology, Pasadena, CA.

Gelbard F. and Seinfeld J. H. (1980) Simulation of multicomponent aerosol dynamics. *J. Colloid Interface Sci.* **78,** 485–501.

Gelbard F., Tambour Y. and Seinfeld J. H. (1980) Sectional representation for simulating aerosol dynamics. *J. Colloid Interface Sci.* **76,** 541–556.

Gery M. W., Fox D. L., Jeffies H. E., Stockburger L. and Weathers W. S. (1985) A continuous stirred tank reactor investigation of the gas phase reaction of hydroxyl radicals and toluene. *Int. J. chem. Kinet.* **17,** 931–955.

Gery M. W., Fox D. L., Kamens R. M. and Stockburger L. (1987) Investigation of hydroxyl radical reactions with *o*-xylene and *m*-xylene in a continuous stirred tank reactor. *Envir. Sci. Technol.* **21,** 339–348.

Gray H. A., Cass G. R., Huntzicker J. J., Heyerdahl E. K. and Rau J. A. (1986) Characteristics of atmospheric organic and elemental carbon particle concentrations in Los Angeles. *Envir. Sci. Technol.* **20,** 580–589.

Grosjean D. (1977) In ozone and other photochemical oxidants. National Academy of Sciences, National Research Council, Washington, DC.

Grosjean D. and Friedlander S. K. (1980) Formation of organic aerosols from cyclic olefins and diolefins. *Adv. Envir. Sci. Technol.* **9,** 435–473.

Grosjean D and Fung K. (1984) Hydrocarbons and carbonyls in Los Angeles air. *J. Air Pollut. Control Ass.* **34,** 537–543.

Harrison R. M. and Pio C. A. (1983) Size-differentiated composition of inorganic atmospheric aerosols of both marine and polluted continental origin. *Atmospheric Environment* **17,** 1733–1738.

Hatakeyama S., Ohno M., Weng J., Takagi H. and Akimoto H. (1987) Mechanism for the formation of gaseous and particulate products from ozone–cycloalkene reaction in air. *Envir. Sci. Technol.* **21,** 52–57.

Hatakeyama S., Tanonaka T., Weng J., Bandow H., Takagi H. and Akimoto H. (1985) Ozone–cyclohexene reaction in air: quantitative analysis of particulate products and reaction mechanism. *Envir. Sci. Technol.* **19,** 935–942.

Hidy G. M., Appel B. R., Charlson R. J., Clark W. E., Friedlander S. K., Hutchison D. H., Smith J. B., Suder J., Wesolowski J. J. and Whitby K. J. (1975). Summary of the California aerosol characterization experiment. *J. Air Pollut. Control Ass.* **25,** 1106–1114.

Hildemann L. M., Russell A. G. and Cass G. R. (1984) Ammonia and nitric acid concentrations in equilibrium with atmospheric aerosols: experiment vs theory. *Atmospheric Environment* **18,** 1737–1750.

Hindmarsh A. C. and G. D. Byrne (1975) EPISODE. An experimental package for the integration of systems of ordinary differential equations, UCID-30112, L.L.L.

Ho W., Hidy G. M. and Govan R. M. (1974) Microwave measurements of the liquid water content of atmospheric aerosols. *J. appl. Met.* **13,** 871–879.

Izumi K., Murano K., Mizuochi M. and Fukuyama T. (1988) Aerosol formation by the photooxidation of cyclohexene in the presence of nitrogen oxides. *Envir. Sci. Technol.* (in press).

Ku J. Y., Rao S. T. and Rao K. S. (1987) Numerical simulation of air pollution in urban areas: model performance. *Atmospheric Environment* **21,** 213–232.

Leone J. A. and Seinfeld J. H. (1984) Analysis of the characteristics of complex chemical reaction mechanisms: application to the photochemical smog chemistry. *Envir. Sci. Technol.* **18,** 280–287.

McRae G. J., Goodin W. R. and Seinfeld J. H. (1982a) Development of a second generation mathematical model for urban air pollution—I. Model formulation. *Atmospheric Environment* **16,** 679–696.

McRae, G. J., Goodin W. R. and Seinfeld J. H. (1982b) Numerical solution of the atmospheric diffusion equation for chemically reacting flows. *J. comput. Phys.* **45,** 1–42.

Niki H., Maker P., Savage C. M. and Breitenbach L. P. (1983) Atmospheric ozone–olefin reactions. *Envir. Sci. Technol.* **17,** 312A–322A.

O'Brien R. J. Holmes J. R. and Bockian A. H. (1975) Formation of photochemical aerosol from hydrocarbons. Chemical reactivity and products. *Envir. Sci. Technol.* **9,** 568–576.

Pilinis C. and Seinfeld J. H. (1987) Continued development of a general equilibrium model for inorganic multicomponent atmospheric aerosols. *Atmospheric Environment* **21,** 2453–2466.

Pilinis C., Seinfeld J. H. and Seigneur C. (1987) Mathematical modeling of the dynamics of multicomponent atmospheric aerosols. *Atmospheric Environment* **21,** 943–955.

Rao S. T., Sistla G., Pagnotti V., Petersen W. B., Irwin J. S. and Turner D. B. (1985) Evaluation of the performance of RAM with the regional air pollution study database. *Atmospheric Environment* **19,** 229–245.

Russell A. G., McCue K. F. and Cass G. R. (1988) Mathematical modeling of the formation of nitrogen-containing air pollutants—I. Evaluation of a Eulerian photochemical model. *Envir. Sci. Technol.* **22,** 263–271.

Saxena P., Hudischewskyj A. R., Seigneur C. and Seinfeld J. H. (1986) A comparative study of equilibrium approaches to the chemical characterization of secondary aerosols. *Atmospheric Environment* **20,** 1471–1483.

Schwartz W. (1974) Chemical characterization of model aerosols. EPA-650/3-74-011. Battelle Memorial Institute, Columbus, OH.

Seinfeld J. H. (1986) *Atmospheric Chemistry and Physics of Air Pollution.* John Wiley, New York.

Seinfeld J. H., Flagan R. C., Petti T. B., Stern J. E. and Grosjean D. (1987) Aerosol formation in aromatic/NO_x systems. Coordinating Research Council Project No. AP-6 Final Report.

Wall S. M., John W. and Ondov J. L. (1988) Measurements of aerosol size distributions for nitrate and major ionic species. *Atmospheric Environment* **22,** 1649–1656.

Warren D. R. and Seinfeld J. H. (1985) Simulation of aerosol size-distribution evolution in systems with simultaneous nucleation, condensation and coagulation. *Aerosol Sci. Technol.* **4,** 31–43.

Wolff G. T. and Klimisch R. L. (1982) *Particulate Carbon. Atmospheric Life Cycle*, p. 297. Plenum Press, New York.